Dalton Transactions

PAPER

Cite this: *Dalton Trans.*, 2014, **43**, 17145

Synthesis, characterization, and reactivity studies of a water-soluble bis(alkoxo)(carboxylato)-bridged diMn^{III} complex modeling the active site in catalase†‡

Claudia Palopoli,[a] Carine Duhayon,[b,c] Jean-Pierre Tuchagues[b,c] and Sandra Signorella*[a]

Received 25th June 2014,
Accepted 18th September 2014

DOI: 10.1039/c4dt01907e

www.rsc.org/dalton

A new diMn^{III} complex, Na[Mn_2(5-SO_3-salpentO)(μ-OAc)(μ-OMe)(H_2O)]·4H_2O, where 5-SO_3-salpentOH = 1,5-bis(5-sulphonatosalicylidenamino)pentan-3-ol, has been prepared and characterized. ESI-mass spectrometry, paramagnetic ^{1}H NMR, EPR and UV-visible spectroscopic studies on freshly prepared solutions of the complex in methanol and 9 : 1 methanol–water mixtures showed that the compound retains the triply bridged bis(μ-alkoxo)(μ-acetato)Mn_2^{3+} core in solution. In the 9 : 1 methanol–water mixture, slow substitution of acetate by water molecules took place, and after one month, the doubly bridged diMn^{III} complex, [Mn_2(5-SO_3-salpentO)(μ-OMe)(H_2O)$_3$]·5H_2O, formed and could be characterized by X-ray diffraction analysis. In methanolic or aqueous basic media, acetate shifts from a bridging to a terminal coordination mode, affording the highly stable [Mn_2(5-SO_3-salpentO)(μ-OMe)(OAc)]$^-$ anion. The efficiency of the complex in disproportionating H_2O_2 depends on the solvent and correlates with the stability of the complex (towards metal dissociation) in each medium: basic buffer > aqueous base > water. The buffer preserves the integrity of the catalyst and the rate of O_2 evolution remains essentially constant after successive additions of excess of H_2O_2. Turnovers as high as 3000 mol H_2O_2 per mol of catalyst, without significant decomposition and with an efficiency of k_{cat}/K_M = 1028 M^{-1} s^{-1}, were measured for the complex in aqueous buffers of pH 11. Kinetic and spectroscopic results suggest a catalytic cycle that runs between Mn^{III}_2 and Mn^{IV}_2 oxidation states, which is consistent with the low redox potential observed for the Mn^{III}_2/$Mn^{III}Mn^{IV}$ couple of the catalyst in basic medium.

Introduction

Nature has developed catalase enzymes to catalyze the redox disproportionation of H_2O_2 into O_2 and H_2O at reasonable rates. Mn-containing catalases (MnCAT) are widespread among prokaryotes and have been isolated from bacteria (*T. thermophilus*,[1] *T. album*,[2] *T.* sp YS 8–13[3] and *L. plantarum*,[4] a hyperthermophilic archeon (*P. caldifontis*[5])) and some cyanobacteria.[6] All known MnCAT enzymes share an unusual Mn_2(μ-O_2CR)(μ-O/OH/H_2O)$_2$ unit that serves as the active site to perform the efficient two-electron disproportionation of H_2O_2, at rates ranging from 2.6 × 10^4 to 2.6 × 10^5 s^{-1}.[7,8] Mechanistic studies performed on biomimetic model compounds provide some clues on the role played by the ligands bridging the Mn ions and the protein environment surrounding the diMn centre during catalysis and contribute to designing efficient low molecular weight catalytic scavengers of H_2O_2 for the prevention of oxidative stress injuries.[9–12]

In aqueous media, the proton coupled disproportionation of H_2O_2 catalyzed by the diMn unit – of either the enzyme or a low-molecular-weight mimic – is strongly affected by pH, which in turn affects the lability of both terminal and bridging ligands, key features of CAT activity.[5,12–14] However, among the large number of Mn-based complexes that have been investigated as low-molecular-weight catalytic scavengers of H_2O_2, only a few Mn complexes have been tested in water,[15–21] most of them being mononuclear complexes which decompose

[a]*IQUIR (Instituto de Química Rosario), CONICET, Facultad de Ciencias Bioquímicas y Farmacéuticas, Universidad Nacional de Rosario, Suipacha 531, (S2002LRK) Rosario, Argentina. E-mail: signorella@iquir-conicet.gov.ar; Fax: +54 341 4350214; Tel: +54 341 4350214 ext: 122*
[b]*LCC (Laboratoire de Chimie de Coordination), 205, route de Narbonne, F-31077 Toulouse, France*
[c]*Université de Toulouse, UPS, INPT, LCC, F-31077 Toulouse, France*

† Dedicated to Prof. Jean-Pierre Tuchagues in memoriam.

‡ Electronic supplementary information (ESI) available: Negative mode ESI-Mass spectra of **1**, UV-vis spectra in H_2O at different times, ^{1}H NMR of **1** in D_4-methanol + D_2O and +D_3-NaOAc, O_2 evolution curves for **1** + H_2O_2 in DMF. CCDC 1008329. For ESI and crystallographic data in CIF or other electronic format. See DOI: 10.1039/c4dt01907e

H_2O_2 after a lag period (the active catalyst is generated during the reaction).[12,16,17,19,21] Therefore, there is a need to obtain MnCAT mimics that are stable in an aqueous medium.

SalpentOH (1,5-bis(salicylidenamino)pentan-3-ol) and its phenyl-ring substituted derivatives afford complexes with a bis(μ-alkoxo)(μ-carboxylato) triply bridged dimanganese(III) core which are structural mimics of the Mn^{III}_2 form of MnCAT.[12] In the present work we employ a water soluble salpentOH derivative, 1,5-bis(5-sulphonatosalicylidenamino)-pentan-3-ol (5-SO_3-salpentOH), to model the geometrical motif of the active site of MnCAT, and analyze the effect of pH on the lability of ligands and catalase activity of the resulting complex, $Na[Mn_2(5\text{-}SO_3\text{-salpentO})(\mu\text{-OAc})(\mu\text{-OMe})(H_2O)]\cdot 4H_2O$ (**1**), in aqueous medium. The kinetic results are compared with those of the diMn complex of the 3-Me,5-SO_3-salpentOH derivative[20] with the target of evaluating the magnitude of the effect of the methyl ring-substituent upon diMn complex reactivity towards H_2O_2 in an aqueous base.

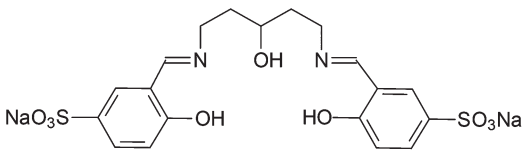

$Na_2[5\text{-}SO_3\text{-salpentOH}]$

Results and discussion

Solid state characterization of 1 and crystal structure of $[Mn_2(5\text{-}SO_3\text{-salpentO})(\mu\text{-OMe})(H_2O)_3]\cdot 5H_2O$ (2)

Complex **1**, $Na[Mn_2(5\text{-}SO_3\text{-salpentO})(\mu\text{-OAc})(\mu\text{-OMe})(H_2O)]\cdot 4H_2O$, was prepared from 1 : 2 mixtures of the ligand with $Mn(OAc)_3\cdot 2H_2O$ in methanol. When $Mn(ClO_4)_2$ was used instead of acetate, no colour change was observed until NaOAc was added to the reaction mixture, to yield the same final complex. In the latter case, acetate facilitates the aerobic oxidation of Mn^{II} besides favouring deprotonation of the alcohol and phenol groups for coordination to the metal, to yield **1**.[22] Although the disodium salt of the ligand was used, conductivity measurements and analytical results show that the complex retains only one sodium ion per molecule in the solid state, and the thermogravimetric analyses indicate that only one of the water molecules is coordinated to the metal centre of each complex. The remaining coordination position of the Mn ion is probably occupied by the sulphonato group of an adjacent complex molecule. The IR spectrum of complex **1** (Fig. 1) shows absorption peaks at 1557 and 1420 cm^{-1} that identify the antisymmetrical and symmetrical stretching vibrations of the *syn–syn* 1,3-bridging acetate,[23] and strong imino and phenolato absorptions at 1616 and 1542 cm^{-1} that are shifted by ≈30 cm^{-1} from those in the free ligand due to the coordination of the metal to these groups. The two strong bands at 1112 and 1034 cm^{-1} are attributable to the antisymmetric and symmetric stretching modes of the $-SO_3^-$ groups. Comparison of the FT-IR spectrum

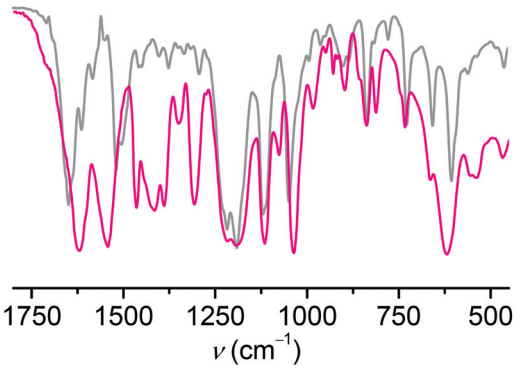

Fig. 1 FT-IR spectra of Na[5-SO_3-salpentOH] (gray) and complex **1** (pink).

of **1** with those of other $diMn^{III}$ complexes of the X-salpentOH family[20,24–28] evidences the fingerprint pattern of the Schiff-base ligand and $\mu_{1,3}$-carboxylato coordinated to the Mn ions.

Complex **1** is stable in methanol and in 9 : 1 methanol–water mixtures, where the complex retains acetate and nuclearity, at least for several hours after preparing the solution (see NMR and ESI-MS results below). However, in this solvent mixture, slow substitution of acetate by water molecules takes place, and after one month $[Mn_2(5\text{-}SO_3\text{-salpentO})(\mu\text{-OMe})(H_2O)_3]\cdot 5H_2O$ (**2**) crystallized and could be characterized by X-ray diffraction analysis.

Compound **2** crystallizes in the $P\,2_1\,2_1\,2_1$ space group with the asymmetric unit containing a dinuclear complex molecule and five solvate water molecules. The molecular structure of complex **2** is illustrated in Fig. 2. In the complex, 5-SO_3-salpentO^{5-} is fully deprotonated and acts as a pentadentate chelating ligand through the N_2O_3 donor set, with one of the sulphonato groups (S2-O12) terminally bound to the Mn1 of a neighbour complex molecule. The two Mn atoms are six-coordinated and doubly bridged by the central alkoxo group of the ligand and one exogenous methoxo ligand. The phenoxo oxygen, imino nitrogen and alkoxo oxygen atoms of the ligand and the methoxo oxygen atom form a meridional geometry around each Mn. The two axial positions of Mn2 are occupied by two coordinated water molecules, while Mn1 is axially coordinated to one water molecule and one oxygen atom of the sulphonato group of an adjacent complex molecule. Inspection of Table 2 shows that both Mn atoms are in an axially elongated octahedral environment, with the Mn1–O7, Mn1–O12, Mn2–O5 and Mn2–O6 bond distances (av. 2.272 Å) distinctly longer than the equatorial Mn1–O1, Mn1–O2, Mn1–O4, Mn2–O2, Mn2–O3, Mn2–O4, Mn1–N1 and Mn2–N2 ones (av. 1.924 Å), which is consistent with the expected Jahn–Teller distortion of the coordination of a d^4 Mn^{III} ion in an octahedral ligand field. The values of the *trans*-angles in the coordination environment of each Mn ion are between 172 and 175° (Table 2), also indicating a distortion from pure octahedral geometry. The Mn···Mn separation of 2.9721(15) Å is in the range observed for other bis(μ-alkoxo)Mn^{III}_2 complexes with axial elongation perpendicular to the bridging plane,[29,30]

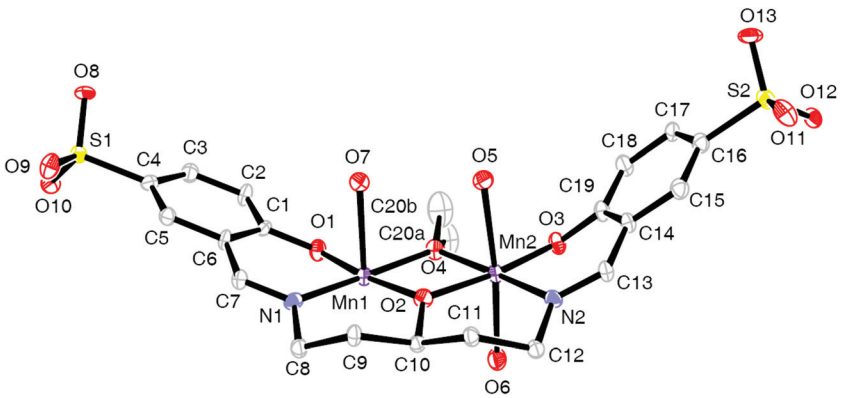

Fig. 2 Asymmetric unit of **2** with atom numbering.

Table 1 Crystal data for $[Mn_2(5\text{-}SO_3\text{-salpentO})(\mu\text{-MeO})(H_2O)_3]\cdot 5H_2O$ (**2**)

Empirical formula	$C_{20}H_{36}Mn_2N_2O_{18}S_2$
M	766.51
Temperature	180 K
Wavelength	0.71073 Å
Crystal system, space group	Orthorhombic, $P212121$
Unit cell dimensions	a = 8.160(5) Å, α = 90.000(5)°
	b = 21.760(5) Å, β = 90.000(5)°
	c = 17.609(5) Å, γ = 90.000(5)°
V	3127(2) Å^3
Z, ρ_{calc}	4, 1.628 Mg m^{-3}
$\mu_{MoK\alpha}$	1.020 mm^{-1}
$F(000)$	1584
Crystal size	0.12 × 0.12 × 0.015 mm
θ range for data collection	2.20 to 26.03°
Limiting indices	$-9 \le h \le 10$, $-26 \le k \le 26$,
	$-21 \le l \le 21$
Reflections collected/unique	24786/6098 [R(int) = 0.0773]
Completeness to θ = 26.03	99.3%
Refinement method	Full-matrix least-squares on F^2
Data/restraints/parameters	6098/2/376
Goodness-of-fit on F^2	1.001
Final R indices [$I > 2\sigma(I)$]	R_1 = 0.0592, wR_2 = 0.1430
R indices (all data)	R_1 = 0.0905, wR_2 = 0.1650
Absolute structure parameter	0.45(3)
Largest diff. peak and hole	1.179 and −0.685 e Å^{-3}

Table 2 Selected bond lengths and angles for compound **2**

Bond lengths (Å)			
Mn1–O1	1.849(5)	Mn2–O2	1.937(5)
Mn1–O2	1.938(5)	Mn2–O3	1.858(5)
Mn1–O4	1.926(5)	Mn2–O4	1.923(5)
Mn1–O12	2.266(5)	Mn2–O5	2.329(5)
Mn1–O7	2.295(5)	Mn2–O6	2.198(6)
Mn1–N1	1.975(6)	Mn2–N2	1.985(6)
Angles (°)			
O1–Mn1–O4	93.5(2)	O3–Mn2–O4	95.2(2)
O1–Mn1–O2	172.5(2)	O3–Mn2–O2	173.5(2)
O4–Mn1–O2	79.26(19)	O4–Mn2–O2	79.4(2)
O1–Mn1–N1	92.9(2)	O3–Mn2–N2	90.8(2)
O4–Mn1–N1	172.0(2)	O4–Mn2–N2	173.2(2)
O2–Mn1–N1	94.1(2)	O2–Mn2–N2	94.4(2)
O1–Mn1–O12	95.8(2)	O3–Mn2–O6	93.8(2)
O4–Mn1–O12	93.9(2)	O4–Mn2–O6	88.2(2)
O2–Mn1–O12	86.56(19)	O2–Mn2–O6	89.8(2)
N1–Mn1–O12	90.1(2)	N2–Mn2–O6	94.5(2)
O1–Mn1–O7	89.2(2)	O3–Mn2–O5	90.4(2)
O4–Mn1–O7	85.8(2)	O4–Mn2–O5	87.49(19)
O2–Mn1–O7	88.5(2)	O2–Mn2–O5	85.73(19)
N1–Mn1–O7	89.6(2)	N2–Mn2–O5	89.3(2)
O12–Mn1–O7	175.01(18)	O6–Mn2–O5	174.28(19)
Mn2–O2–Mn1	100.2(2)	Mn2–O4–Mn1	101.1(2)

and is markedly shorter than for bis(alkoxo)$Mn^{III}{}_2$ complexes (≈3.2 Å), with the Jahn–Teller elongation axis oriented along the bridging core.[31–35]

Fig. 3 displays the crystal packing of compound **2** along c. In the crystal structure, each dinuclear entity is connected to two adjacent diMn molecules through coordination of Mn(1) and O(12) of the sulphonato group of the basic dinuclear unit to the respective O(12) and Mn(1) from adjacent complex molecules, forming 1-D chains.

The crystal packing reveals that the structure also contains extended hydrogen contacts between sulphonato groups (O8, O9, O11), phenoxo (O3), and coordinated (O5, O7) and crystallized (O14, O15, O16, O17, O18) water molecules. Fig. 4 displays the crystal packing of compound **2** along a. The five crystallographically unique lattice water molecules and their symmetrically related molecules link to each other to form a water grid through hydrogen bonds acting as glue between the polymeric 1-D chains of complex **2**, yielding a 3-D structure.

ESI-mass spectrometry (ESI-MS)

ESI-mass spectra of complex **1** confirm its chemical composition and retention of nuclearity in solution. In methanol, the positive mode ESI mass spectrum of complex **1** (Fig. 5(a)) shows two main peaks at m/z = 727.1 (100%) and 705.2 (59%), which originate from the $Na_2[Mn_2(5\text{-}SO_3\text{-salpentO})(OMe)(OAc)]^+$ and $NaH[Mn_2(5\text{-}SO_3\text{-salpentO})(OMe)(OAc)]^+$ monocations, respectively. Other peaks generated during the electrospray experiments correspond to the substitution of OAc by OMe ($Na_2[Mn_2(5\text{-}SO_3\text{-salpentO})(OMe)_2]^+$, m/z = 677.2, 30%), the exchange of OMe or OAc by OH ($Na_2[Mn_2(5\text{-}SO_3\text{-salpentO})(OMe)(OH)]^+$, m/z = 685.6, 16% and $Na_2[Mn_2(5\text{-}SO_3\text{-salpentO})(OH)(OAc)]^+$, m/z = 713, 14%), and the loss of OAc ($Na_3[Mn_2(5\text{-}SO_3\text{-salpentO})(OMe)]^+$, m/z = 691.2, 15%). The isotopic patterns of these peaks match their simulated spectra very well. When complex **1** is dissolved in a 9 : 1 methanol–water mixture, the major peak of the ESI-mass spectrum also appears at m/z = 727.1 (100%) (Fig. 5(b)), with peaks belonging

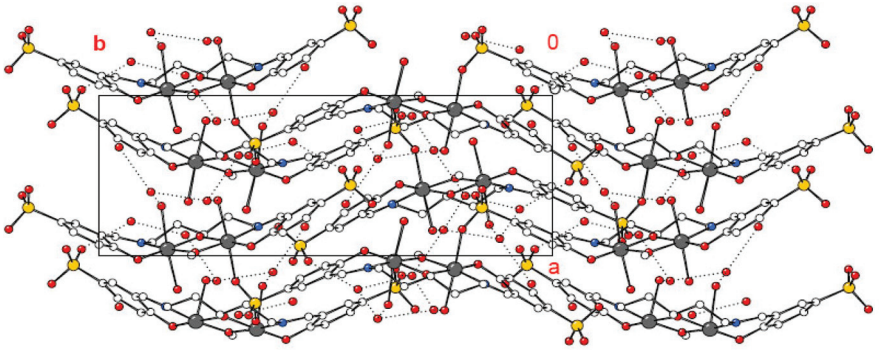

Fig. 3 Packing diagram of **2** viewed along the crystallographic *c*-axis.

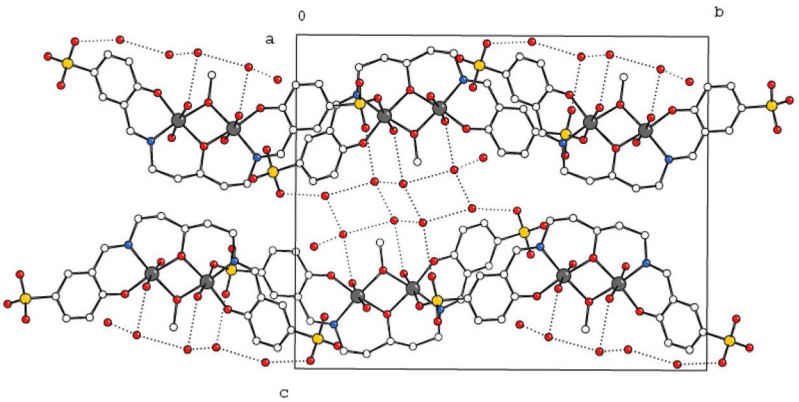

Fig. 4 Packing diagram of **2** viewed along the crystallographic *a*-axis.

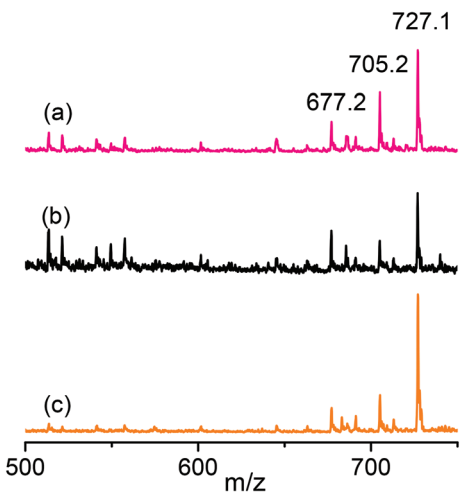

Fig. 5 Positive mode ESI-mass spectra of **1** in (a) methanol, (b) 9 : 1 methanol–H_2O and (c) Et_3N–Et_3NH^+ buffer of pH 11.

to the monocations generated by substitution of the exogenous bridging ligands by hydroxide or methoxide from the solvent ($Na_2[Mn_2(5\text{-}SO_3\text{-salpentO})(OMe)_2]^+$, $Na_2[Mn_2(5\text{-}SO_3\text{-salpentO})(OMe)(OH)]^+$ and $Na_2[Mn_2(5\text{-}SO_3\text{-salpentO})(OH)(OAc)]^+$), also present.

In the Et_3N–Et_3NH^+ buffer of pH 11, even when the ESI-mass spectra are dominated by the peak of the buffer (m/z = 303.5, $[(Et_3NH)_2(ClO_4)]^+$, 100%), monocation $Na_2[Mn_2(5\text{-}SO_3\text{-salpentO})(OMe)(OAc)]^+$ can be well identified as the major species (Fig. 5(c)). Triethylamine adducts ($H(Et_3NH)[Mn_2(5\text{-}SO_3\text{-salpentO})(OMe)(OAc)]^+$, m/z = 784.2, $Na(Et_3NH)[Mn_2(5\text{-}SO_3\text{-salpentO})(OMe)(OAc)]^+$, m/z = 806.1, and $(Et_3NH)_2[Mn_2(5\text{-}SO_3\text{-salpentO})(OMe)(OAc)]^+$, m/z = 885.1) and all other species generated by ligand exchange with the solvent show low relative intensities (<10% of the peak at m/z = 727.1). Identical spectra are obtained several hours after preparation of solutions of **1** in Et_3N–Et_3NH^+ buffer. In addition, negative mode ESI-mass spectra of the complex in either methanol or buffer solution of pH 11 are dominated by the peak at m/z = 681.2 (100%) corresponding to the $[Mn_2(5\text{-}SO_3\text{-salpentO})(OMe)(OAc)]^-$ anion. Other anionic species generated during electrospray show intensities < 15% of the main peak (Fig. S1, ESI‡).

Electronic spectroscopy

The electronic spectrum of complex **1** in H_2O (Fig. S2, ESI‡) exhibits intense absorption bands between 220 and 300 nm, attributed to $\pi\rightarrow\pi^*$ transitions from the ligand. Absorptions in the 300–500 nm range correspond to ligand-centered transitions overlapping with L→M charge-transfer transitions from pπ orbitals of the phenoxo oxygen to the partially filled dπ orbitals of the Mn^{III} ion,[36–39] while the low intensity band at 575 nm (ε = 560 M^{-1} cm^{-1}) can be assigned to a d–d transition

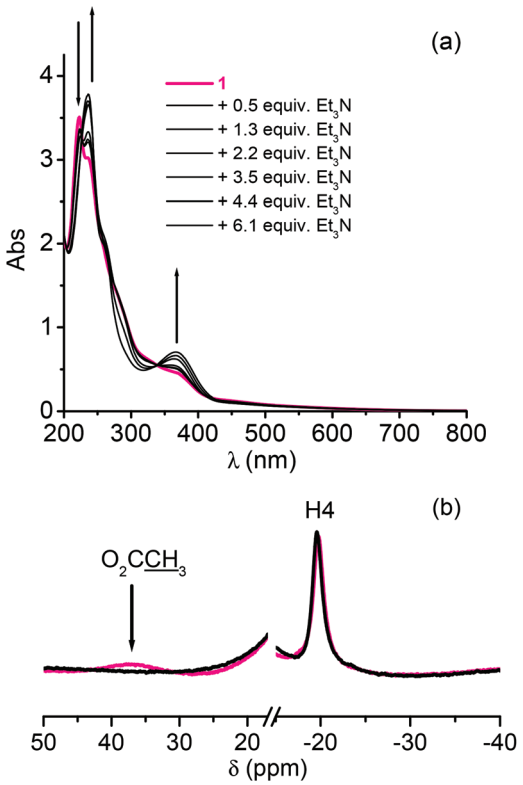

Fig. 6 (a) Electronic spectra of **1** in water before (pink) and after (black) addition of increasing amounts of Et_3N. [**1**] = 6.5 × 10^{-2} mM. (b) ^1H NMR spectra of **1** (20 mM), before (pink) and after (black) the addition of 5.0 equiv. of Et_3N, in D_4-methanol.

in agreement with reported values for related $diMn^{III}$ complexes.[11,37,38,40,41]

With time, absorbance at 270 nm decreases and the band at 228 nm splits into two bands at 222 and 234 nm, due to sulphonate protonation. This acid–base process occurs with an isosbestic point at 307 nm. Aqueous solutions of Na_2[5-SO_3-salpentOH] exhibit similar behaviour. Concurrently, partial metal dissociation also contributes to the observed spectral changes (see below). The final equilibrium is reached in about 4 h, and the stabilized spectrum of **1** is shown in Fig. 6(a) (pink line). Addition of Et_3N to the aqueous solution of the complex re-establishes the band at 270 nm and results in an intense absorption at 370 nm due to intraligand transitions of the sulphonato ligand superimposed to phenolate to Mn^{III} CT transitions (Fig. 6(a), black lines). The intensity of this absorption grows linearly with increasing concentrations of Et_3N. In Et_3N–Et_3NH^+ buffer of pH 11, the molar absorption coefficient of this band is 1.41 times higher than for the free ligand and can be used to monitor the integrity of the complex during H_2O_2 disproportionation in basic solution.

^1H NMR spectroscopy

The paramagnetic ^1H NMR spectrum of **1** in D_4-methanol (Fig. 6(b), pink line) shows a simple pattern for this complex, containing two proton resonances that lie outside the diamagnetic region (δ = 0–14). The upfield resonance, observed at −19.5 ppm, can be assigned to the H4 proton of **1**,[42–45] while the broad resonance at 38 ppm may be attributed to the methyl group of the bridging acetato of **1** on the basis of comparison with the spectra of other Mn^{III}_2-μ-OAc complexes studied previously.[43,44] This assignment was confirmed by addition of D_3-NaAcO to the solution of **1** in D_4-methanol, which resulted in the disappearance of the broad resonance at 38 ppm (Fig. S3, ESI‡). Due to their closeness to the Mn, the resonance of protons *ortho* to the donor groups of the Schiff base ligand (H3 and H6) are probably too broad to be observed.[42–45] The signal of the bridging acetato persisted upon addition of up to 10% D_2O to the methanolic solution of the complex (Fig. S4, ESI‡). Conversely, solutions of **1** in neat D_2O showed a unique low intensity resonance for the aromatic proton, indicating partial metal dissociation (see below).

Addition of 5 equiv. of Et_3N to the D_4-methanol solution of **1** causes disappearance of the bridging acetate protons resonance, while that from H4 of the Schiff base ligand remains unchanged (Fig. 6(b), black line). The unchanging paramagnetic shift of the ligand proton indicates that the magnetic coupling between Mn ions is the same as in starting **1**. Besides, the ESI-MS results described above showed that in methanol–Et_3N the complex retains acetate. Therefore, the disappearance of the broad resonance corresponding to the acetate protons, together with the unchanged chemical shift of the aromatic proton, points to the conversion of the bridging acetato into a monodentate terminal ligand, the chemical shift of which is within the diamagnetic region of the spectrum.[46] The ^1H NMR spectrum obtained in basic medium also excludes the formation of an oxo-bridged Mn^{III}_2 that should provide a better exchange pathway between Mn ions, affording a spectrum with a H4 paramagnetic shift different from that of the starting compound.[42,46–49] Therefore, the basic medium prevents the complex from dissociation.

Kinetic stability of the complexes

Complex **1** is EPR silent in the solid state and in frozen MeOH solution ($T \approx 110$ K), a fact consistent with the presence of Mn^{III} ions. However, when **1** is dissolved in water, a 6-line EPR signal (hyperfine splitting of ≈90 G) with $g \approx 2$ characteristic of an Mn^{2+}_{aq} ion is observed (Fig. 7, red line), meaning that water induces dissociation of the metal ion from the complex. Double integration of EPR spectra of the complex in water and comparison against Mn(II) standard indicates 10% of Mn^{2+}_{aq} in solution. When the complex solution is prepared in basic aqueous solution (by either addition of Et_3N or preparing the solution in a buffer of pH = 11), the solution is EPR silent even after 24 h (Fig. 7, blue line), meaning that the exogenous base prevents complex dissociation in water. The stability of complex **1** in aqueous basic medium was also checked by UV-vis spectroscopy. Spectra of the complex registered at different time-lengths after preparation of solutions **1** in either Et_3N–Et_3NH^+ buffer of pH 11 or Et_3N–H_2O (pH = 10.75), showed identical λ_{max} and molar absorbance coefficients.

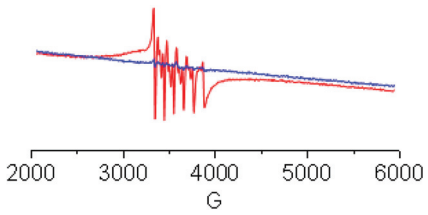

Fig. 7 EPR spectra taken 24 h after preparing solutions of **1** in H_2O (red) and buffer of pH 11 (blue); ν = 9.5 GHz, T = 100 K, and microwave power = 0.5 mW.

Electrochemistry

In methanol, the complex exhibits one quasi-reversible reduction wave at $E_{1/2}$ 167 mV (Fig. 8(a)), which can be attributed to the $Mn^{III}{}_2/Mn^{III}Mn^{II}$ redox couple as confirmed by linear voltammetry and square-wave voltammetry ($W_{1/2}$ = 135 mV) experiments. An additional nonreversible reduction peak was observed at $E_c \approx -650$ mV attributable to the Mn^{III}-$Mn^{II}/Mn^{II}{}_2$, in accordance with previously reported complexes with a similar environment.[25–28]

After addition of Et_3N to the MeOH solution of **1**, $Mn^{III}{}_2/Mn^{III}Mn^{II}$ and $Mn^{III}Mn^{II}/Mn^{II}{}_2$ reduction processes take place at 150 and ~ −500 mV. Upon oxidation, the cyclic voltammogram of **1** shows one additional reversible anodic process at $E_{1/2}$ 445 mV (Fig. 8(b)). A plausible explanation for the appearance of this wave, only observed in basic medium, is that it results from oxidation of the form in which solvent (or base) binds the metal through acetate-shift (from bridging to terminal position) to yield (S)$Mn^{III}{}_2$-OAc.[41,42] This ligand-shift affects the cathodic wave slightly, but lowers the potential of the $Mn^{III}Mn^{IV}/Mn^{III}{}_2$ couple, bringing closer the two redox couples of **1**. This result is consistent with the ^{1}H NMR results. An irreversible peak at $E_a \approx 850$ mV is also observed in the oxidative scan, but it was already present in the voltammogram of the Et_3N–MeOH mixture.

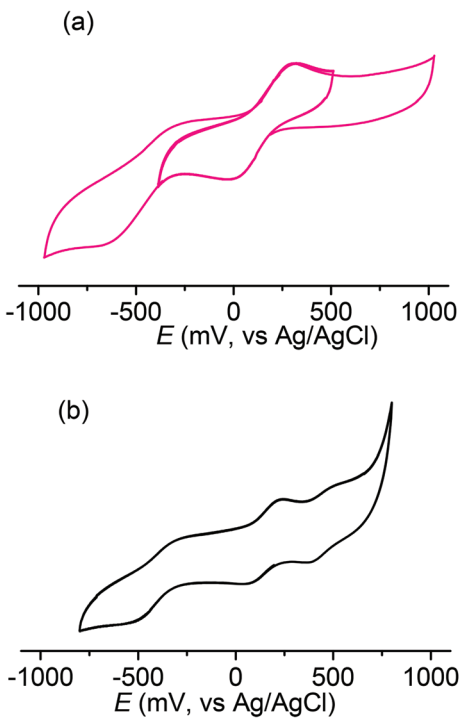

Fig. 8 Cyclic voltammograms of (a) **1** and (b) **1** + 5 equiv. Et_3N, in methanol. [**1**] = 1 mM. Supporting electrolyte = Bu_4NPF_6. Scan rate = 100 mV s^{-1}, working electrode = glassy carbon.

H_2O_2 dismutation studies

The ability of complex **1** to catalyze H_2O_2 disproportion was first tested in H_2O. Addition of H_2O_2 to an aqueous solution of the catalyst caused an immediate vigorous evolution of O_2. The volumetric measurement of evolved O_2 reveals that in this solvent **1** is able to catalyze the decomposition of H_2O_2, but after successive additions of excess H_2O_2 to the catalyst solution the rate of O_2 formation gradually decreases (Fig. 9(a)). Electronic spectra registered immediately after addition of 150 equiv. H_2O_2 show that the band at 362 nm increases and red shifts to 382 nm. Then, during the progress of the reaction, this band decreases and blue shifts concurrently with the growth of the band at 326 nm, with an isosbestic point at 343 nm (Fig. 9(b)). EPR spectra taken during the reaction show a six line signal typical of $Mn^{2+}{}_{aq}$ (Fig. 9(c)) which accumulates in the reaction mixture irreversibly.

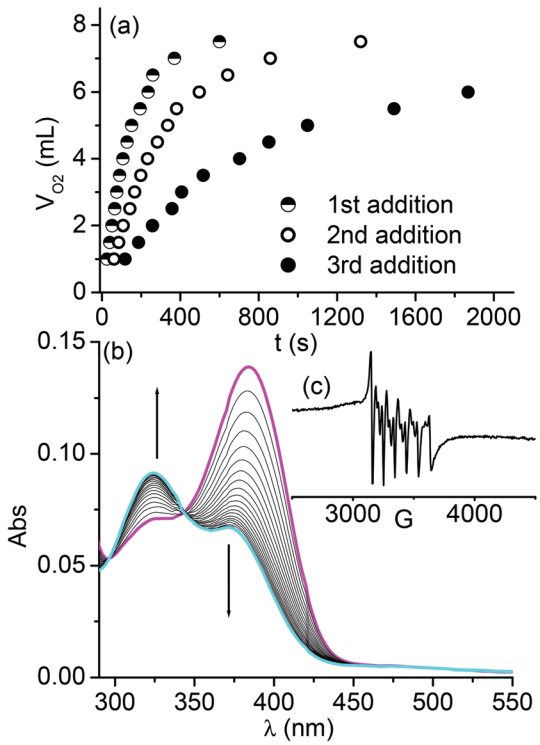

Fig. 9 (a) Volume of O_2 evolved after three successive additions of 130 equiv. H_2O_2 to an aqueous solution of **1** (1.56 × 10^{-3} M). T = 298 K. (b) Electronic spectra registered after addition of 150 equiv. H_2O_2 to an aqueous solution of **1** (1.4 × 10^{-5} M). (c) EPR spectrum taken at the end of disproportionation of 150 equiv. of H_2O_2 by **1** in water; ν = 9.5 GHz, T = 100 K, and microwave power = 0.5 mW.

In order to find a better solvent for disproportionation of H_2O_2 by complex **1**, DMF, a nonprotic solvent, and basic Et_3N aqueous solution were essayed. In DMF, O_2 evolution starts after a lag period, which stretches on a second addition of 130 equiv. of H_2O_2 to the solution of **1** (Fig. S5, ESI‡). After six additions of excess of H_2O_2, the catalyst retrieves its initial activity and the lag period shortens to a time close to the starting value. Higher amounts of H_2O_2 added to the reaction mixture show kinetic traces similar to, or even faster than, that of the first addition, probably because a new active form of the catalyst is generated in this solvent.

In basic aqueous medium, **1** is a better catalyst than in neat water. However, after successive additions of excess of H_2O_2 to a solution of **1** in Et_3N–H_2O, the rate of O_2 evolution decreases gradually as do the absorption bands in the electronic spectra of the complex after each new addition of H_2O_2 (Fig. 10). Changes in the intensity of the spectral bands of **1** are the same as observed when lowering the pH. Simultaneously, a six lines EPR signal due to aqueous Mn^{2+} ion builds up and persists at the end of the reaction, indicating partial dissociation of the complex during the catalytic cycles. Thus, when the reaction is performed in aqueous Et_3N, as base equivalents are consumed, protonation of the catalyst results in metal dissociation with concomitant loss of CAT activity.

The performance of the catalyst could be improved by employing buffered aqueous solutions. It was found that pH must be controlled to values >8.5 for the catalyst to retain its activity after successive additions of H_2O_2. Turnovers as high as 3000 (mol H_2O_2/mol catalyst) without significant decomposition were measured for the complex in buffer Et_3N–Et_3NH^+ of pH 11. As shown in Fig. 11(a,b), the rate of O_2 evolution remains essentially constant after successive additions of 150 equiv. of H_2O_2, with no changes in the electronic spectra of **1**.

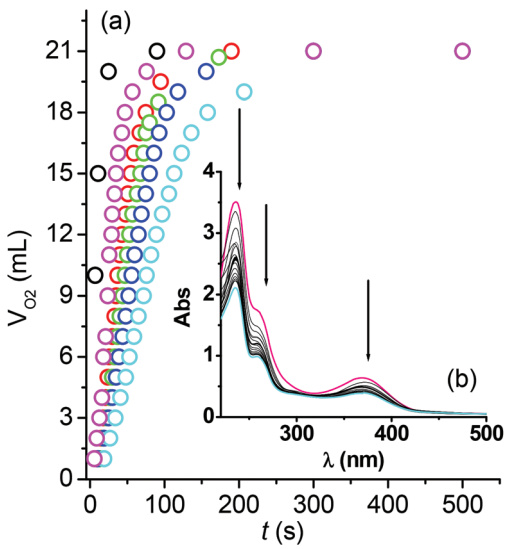

Fig. 10 (a) Time-dependence of O_2 evolution after successive additions of 145 μL of 10.49 M H_2O_2 (375 equiv.) to an aqueous solution of **1** (1.44 mM) + 10 equiv. Et_3N; (b) Electronic spectra registered after successive additions of 150 equiv. H_2O_2 to the aqueous solution of **1** (6×10^{-5} M) + 10 equiv. Et_3N. T = 298 K.

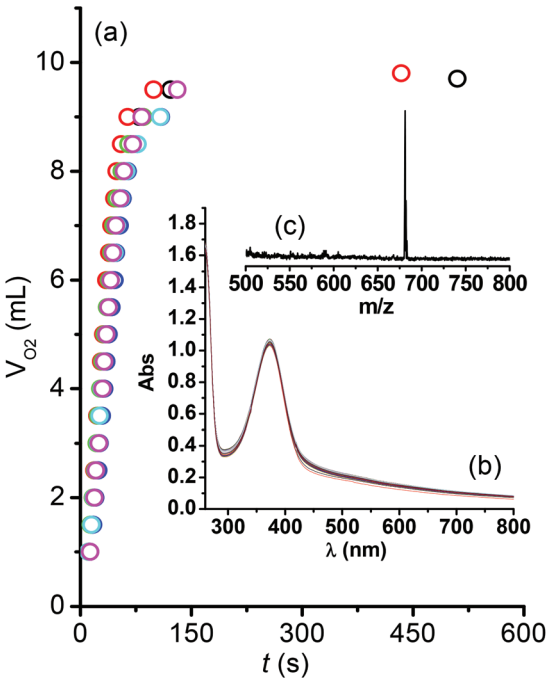

Fig. 11 (a) Time-dependence of O_2 evolution after successive additions of 150 equiv. H_2O_2 to an aqueous solution of **1** (1.73 mM) in buffer at pH 11. (b) Electronic spectra registered after successive additions of 160 equiv. H_2O_2 to the solution of **1** (6.5×10^{-5} M) in buffer at pH 11. (c) Negative mode ESI-mass spectrum registered on a mixture of **1** + 150 equiv. of H_2O_2 in buffer at pH 11. T = 298 K.

Under these conditions, the reaction mixture is EPR silent, meaning that the buffer prevents metal dissociation during catalysis. Besides, the absence of EPR signal during the reaction course suggests that the Mn^{III}_2 form of the catalyst is the main species in solution since no EPR signal is expected for the catalyst in this oxidation state. Negative mode ESI-mass spectra taken during and at the end of the reaction show the peak at m/z 681 (Fig. 11(c)), which corresponds to the $[Mn_2(5\text{–}SO_3\text{–salpentO})(OMe)(OAc)]^-$ anion, indicating that the catalyst retains nuclearity and composition during catalysis.

Kinetics

The initial rate of H_2O_2 disproportionation by complex **1** in H_2O and in Et_3N–Et_3NH^+ buffer of pH 11.05 was measured as a function of the complex and substrate concentrations at 25 °C. In both media, at constant $[H_2O_2]_0$, the initial rate of H_2O_2 disproportionation varies linearly with the $[catalyst]_0$, meaning that the reaction is first order with the catalyst. The first order dependence of the reaction rate on the catalyst and the lack of time-lag at the onset of the reaction suggest that the starting complex is responsible for the rapid disproportionation of H_2O_2. At constant $[catalyst]_0$, the initial rate of H_2O_2 dismutation exhibits saturation kinetics with $[H_2O_2]_0$ (Fig. 12), and the experimental data could be fitted to the Michaelis–Menten equation from which the catalytic turnover

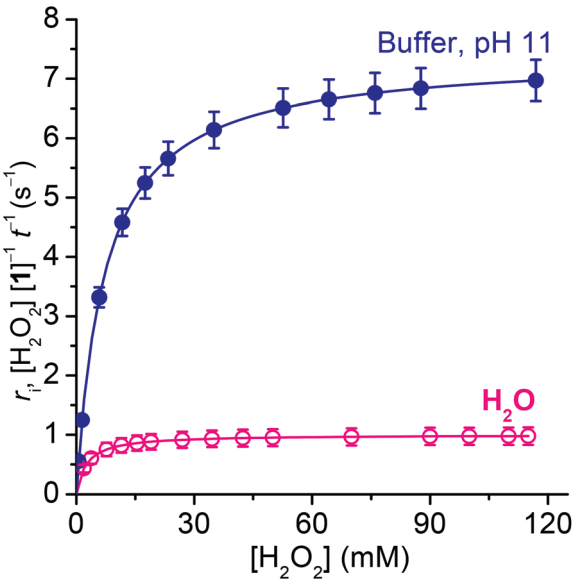

Fig. 12 Effect of the $[H_2O_2]$ on the initial rate of H_2O_2 disproportionation catalyzed by **1**, at 298 K, in water and in an aqueous Et_3N buffer pH 11.05.

number (k_{cat}) and the Michaelis constant (K_M) were determined (Table 3).

Values of k_{cat} measured in either water or basic medium are in the range of those determined for a number of alkoxo-bridged diMn complexes;[9,12] however, based on the k_{cat}/K_M criterion, **1** is much more efficient than most of these complexes. The high efficiency of the present catalyst results from the low value of K_M, which in water is one-sixth of the value found for $[Mn_2(salpentO)(\mu\text{-}OAc)(\mu\text{-}OMe)]^+$ in methanol (Table 3).[28] Decrease of K_M values in the presence of water has also been observed for $[Mn_2(O)_2tpa_2]^{3+}$ (Table 3) and related complexes.[15,50] In the case of **1**, the negative formal charge of the complex and coexistence of H_2O_2 with HO_2^- at pH 11, result in an affinity of the catalyst for the substrate in neat water that is higher than in buffered basic solution (higher affinity of **1** for H_2O_2 *vs.* HO_2^-). Conversely, positively charged complexes have shown to be more efficient at binding the substrate in basic aqueous medium than in water (entries 6 and 7, Table 3).[51] The higher efficiency of **1** (k_{cat}/K_M) in the buffer solution results from turnover numbers (k_{cat}) seven-times larger than in water. Thus, **1** is more effective at oxidizing peroxide but is poorer at binding the substrate in basic aqueous buffer than in water, so a maximal rate in the buffer is achieved at higher $[H_2O_2]$.

Comparison with the methyl-substituted complex, $[Mn_2(\mu\text{-}OMe)(\mu\text{-}OAc)(3\text{-}Me,5\text{-}SO_3\text{-}salpentO)]^-$ (**3**), provides information on the oxidation states of Mn involved in the catalytic cycle. Complex **3** with an electron-donor substituent, is a better reducing agent (electron-donor effect stabilizes higher oxidation states) and has higher k_{cat} (Table 3).[20] The fact that catalyst **3**, which is easier to oxidize, reacts faster than **1** (H < electron-donor substituent) suggests that oxidation of the catalyst with simultaneous H_2O_2 reduction should be the slow step in the catalytic cycle. This implies that the reduced form of the catalyst is the major catalytic species in solution, which, from the spectroscopic studies, is a Mn^{III}_2 species. Therefore, kinetic and spectroscopic results point to a catalytic cycle that runs between Mn^{III}_2 and Mn^{IV}_2 oxidation states, which is consistent with the low redox potential observed for the Mn^{III}-Mn^{IV}/Mn^{III}_2 couple of **1** in basic medium and the lack of mixed valence and Mn^{II}_2 species in the EPR spectra.

Conclusions

The pentadentate ligand 5-SO_3-salpentOH affords a water-soluble complex with a bis(μ-alkoxo)($\mu_{1,3}$-carboxylato) triple-bridged dimanganese(III) core, a geometric motif similar to that found in the active site of Mn^{III}_2 form of *T. thermophilus*[7] and *L. plantarum*[8] CAT, where the two Mn ions are triply-bridged through a $\mu_{1,3}$-carboxylate from Glu (Glu70[7] and Glu66,[8] respectively) and two solvent-derived single oxygen atom bridges.

Complex **1** retains its chemical composition in methanol solutions, but in neat water, acetate de-coordinates rapidly and metal dissociation occurs. Slow dissociation of acetate occurs in 9 : 1 methanol–water mixtures, where complex **1** transforms into **2** after several weeks, with only a slight amount of free metal ion accumulated in the solution. Addition of a base induces an acetato-shift from bridging to terminal, and prevents acetate and metal hydrolysis in water solution. In basic medium, the complex is stable in solution for a long time.

Table 3 k_{cat} and K_M values for **1** and other dimanganese functional CAT models[a]

Catalyst	k_{cat} (s^{-1})	K_M (mM)	k_{cat}/K_M (s^{-1} M^{-1})	Solvent	Ref.
1	1.0(5)	2.5(8)	400	H_2O	This work
1	7.4(2)	7.2(8)	1028	Buffer pH 11.05	This work
$[Mn_2(salpentO)(\mu\text{-}OAc)(\mu\text{-}OMe)]^+$	0.98(9)	14(5)	70	MeOH	28
$[Mn_2(3\text{–}Me,5\text{–}SO_3\text{–}salpentO)(\mu\text{-}OAc)(\mu\text{-}OMe)]^-$	10.5(2)	6.6(4)	1600	Buffer pH 10.6	20
$[Mn_2(O)_2tpa_2]^{3+}$	107(24)	3100(400)	35	MeCN	15
	1.97(5)	1470(30)	1.3	MeCN–H_2O	
$[Mn_2(\mu\text{-}OAc)(\mu\text{-}OH_2)(benzimpnO)]^{2+}$	2.7(1)	6(4)	450	MeOH–H_2O	51
$[Mn_2(\mu\text{-}OAc)(\mu\text{-}OH_2)(benzimpnO)]^{2+}$ + 5 equiv. OH^-	2.1(1)	3(0.4)	700	MeOH–H_2O	51

[a] BenzimpnOH = *N*,*N*,*N*′,*N*′-tetrakis(2-methylenebenzimidazolyl)-1,3-diaminopropan-2-ol; tpa = tris-2-picolylamine.

Complex **1** proves to be a very efficient CAT mimic in aqueous medium of pH > 8.5 (k_{cat}/K_M = 1028 M^{-1} s^{-1} at pH 11), especially due to its high affinity for the substrate, even higher than the enzyme.[2–4] In this complex, the presence of labile H_2O molecules bound to the Mn ions facilitates H_2O_2 binding through H_2O–H_2O_2 exchange, while the bridges can serve as proton storage sites. Besides, the two Mn ions possess the same NO_5 coordination sphere providing a symmetrical environment that stabilizes the homovalent diMn core and facilitates redox activity based on shuttling between $Mn^{III}{}_2$ and $Mn^{IV}{}_2$ states during disproportionation of H_2O_2.

In the absence of a buffer, catalytic efficiency of complex **1** decreases, especially due to protonation of the bridges and consequent metal dissociation. The pH dependence of the CAT activity of this mimic resembles the behaviour of the enzyme, for which the loss of activity below pH 5 has been proposed to result from protonation of the catalytically active Mn(μ-OR)$_2$Mn closed form of the $Mn^{III}{}_2$ state (the major form at high pH), to yield an inactive H_2OMn(μ-OR)MnOH open form at pH 6.5.[13]

Experimental section

Materials

All reagents or AR chemicals were used as purchased. Solvents were purified by standard methods. The concentration of H_2O_2 stock solution was determined by iodometric titration. Sodium salicylaldehyde-5-sulphonate was prepared according to a published method.[52,53]

Physical measurements

Electronic spectra were recorded on a JASCO V550 spectrophotometer with thermostated cell compartments. IR spectra were recorded on a Perkin-Elmer Spectrum One FT-IR spectrophotometer. ESI-mass spectra were recorded on a Perkin-Elmer SCIEX 365 LCMSMS mass spectrometer. The electrospray solutions were prepared from water, buffer of pH 11 or methanol solutions of the complexes and diluted with methanol to a ≈10^{-5} M concentration at a flow rate of 5 μL min^{-1}. EPR spectra were obtained on a Bruker ESP 300 E spectrometer with a microwave frequency generated with a Bruker ER 04 (9–10 GHz). The microwave frequencies were measured with a Racal-Dana frequency meter and the magnetic field was measured with a Bruker NMR probe Gaussmeter. ^{1}H and ^{13}C NMR spectra were recorded on a Bruker AC 200 NMR spectrometer at ambient probe temperature (*ca.* 26 °C), with nominal operating frequencies of 200.1 and 50.3 MHz. Conductivity measurements were performed using a Horiba F-54 BW conductivity meter, on 1.0 mM solutions of the complexes in water. The electrochemical experiments were performed with a computer-controlled Princeton Applied Research potentiostat, model VERSASTAT II, with model 270/250 Research Electrochemistry Software. Studies were carried out under Ar, in methanol solutions using 0.1 M Bu_4NPF_6 as a supporting electrolyte and ~10^{-3} M of the complex. The working electrode was a glassy carbon disk and the reference electrode was Ag/AgCl with Pt as the auxiliary electrode. All potentials are referred to the Ag/AgCl electrode. Using the described conditions, the ferrocene/ferrocenium redox couple was observed at $E_{1/2}$ = 418 mV in methanol.

Crystal data collection and refinement

Crystallographic data for compound **2** were collected on a Stoe Imaging Plate Diffractometer System (IPDS) equipped with an Oxford Cryosystems cooler device using graphite-monochromated Mo-Kα radiation. Data collection, cell refinement and data reduction were carried out using the Stoe IPDS package.[54,55] The structure was solved by direct methods with SIR 92[56] and refined by full-matrix least-squares on $F_o{}^2$ with SHELXL-97,[57] using anisotropic displacement parameters for non-hydrogen atoms. Hydrogen atoms could not be located on water molecules. The molecular plots were drawn using the Ortep-3 for Windows program[58] with 50% probability displacement ellipsoids. Crystal data collection and refinement parameters are summarized in Table 1. CCDC 1008329 (**2**) contains the supplementary crystallographic data for this paper.

Synthesis of disodium salt of 1,5-bis(5-sulphonatosalicylidenamino)pentan-3-ol (5-SO_3-salpentOH)

Na_2[5-SO_3-salpentOH]·3H_2O was prepared by Schiff-base condensation of sodium salicylaldehyde-5-sulphonate (5.027 g, 22 mmol) with 1,5-diaminopentan-3-ol[59] (11 mmol) in ethanol (100 mL), at reflux for 2 h. Na_2[5-SO_3-salpentOH]·3H_2O was isolated as a pure yellow solid by precipitation from the reaction mixture after 48 h, at room temperature. Yield: 5.415 g (9.27 mmol, 84%). Anal. calcd for $C_{19}H_{20}N_2Na_2O_9S_2$·3$H_2O$: C 39.04, H 4.45; N 4.79; S 10.97. Found: C 39.48; H 4.50; N 4.74; S 10.88. ^{1}H NMR (D_6-DMSO) δ: 8.58 (s, 2H, N=CH–), 7.66 (d, 2H, C6-H), 7.52 (dd, 2H, C4-H), 6.77 (d, 2H, C3-H), 3.68 (m, 1H, *H*–C(OH)–), 2.5 (m, 4H, –C*H*$_2$–N), 1.74 (m, 4H, (HO)C–C*H*$_2$–). ^{13}C NMR (D_2O) δ: 175.52 (Ar), 168.39 (CH=N), 133.92, 132.43, 127.87, 123.75, 114.12 (Ar), 66.95 (R$_2$*C*H–OH), 48.69 (N–CH_2–), 36.01 (–*C*H_2–CHOH–). UV-visible (UV-vis) λ_{max} nm (ε M^{-1} cm^{-1}) in Et_3N–Et_3NH^+ buffer, pH 11: 236 (58 100), 259 (20 200), 370 (11 800). Significant IR bands (KBr, ν cm^{-1}): ν_{OH} 3420 (broad), $\nu_{C=N}$ 1648, ν_{SO3} 1113/1043.

Synthesis of Na[Mn_2(5-SO_3-salpentO)(μ-OAc)(μ-OMe)-(H_2O)]·4H_2O (1)

$Mn(OAc)_3$·2H_2O (0.3914 g, 1.46 mmol) was added to a solution of Na_2[5-SO_3-salpentOH]·3H_2O (0.44 g, 0.75 mmol) in methanol (13 mL). The mixture was stirred for 20 minutes, then filtered and the resulting green solution was left to stir for 24 h. Addition of 80 mL of acetonitrile caused the formation of a green precipitate, which was collected by filtration, washed with methanol and hexane and dried under vacuum. Yield 0.4249 g of **1** (0.54 mmol, 72%). Anal. calcd for $C_{22}H_{25}Mn_2N_2NaO_{13}S_2$·4$H_2O$: C 33.25, H 4.16, Mn 13.85, N 3.53, Na 2.90, S 8.06%; found: C 33.20, H 3.76, Mn 13.5, N 3.55, Na 2.79, S 7.58%. Significant IR bands (KBr, ν cm^{-1}): ν_{OH} 3450, ν_{CH} 2931, 2857, $\nu_{C=N}$ 1616, ν_{AcO} 1557/1420,

ν_{SO3} 1112/1034. UV-vis λ_{max} nm (ε M^{-1} cm^{-1}) in H_2O (immediately after preparation of solution): 229 (53 800), 271 (37 040), 362 (sh, 6524), 443 (1285), 575 (560); in Et_3N–Et_3NH^+ buffer, pH 11: 236 (65 900), 259 (30 950), 370 (16 680); in DMF: 370 (6460), 460 (1160), 597 (368). These absorption bands obey Beer's law over the range of concentrations above 10 μM used in this work. Molar conductivity = 125 Ω^{-1} cm^2 mol^{-1}. The content of 4 molecules of non-coordinated water per complex molecule was confirmed by thermogravimetric analysis of the complex which showed 9.5% mass loss below 120 °C. Single crystals of $[Mn_2(5\text{-}SO_3\text{-}salpentO)(\mu\text{-}OMe)(H_2O)_3]\cdot 5H_2O$ (**2**) suitable for X-ray diffraction were obtained by crystallization from a solution of **1** in a 9 : 1 methanol–H_2O mixture layered with ethyl ether, upon standing in air for about one month.

Volumetric measurements

The stoichiometry of the reaction was measured by volumetric determination of the evolved O_2 from reaction mixtures in DMF, methanol, water, aqueous Et_3N, or buffer Et_3N–$Et_3NH\cdot ClO_4$ of pH = 11. A round-bottom flask with a stopcock-equipped gas delivery side tube connected to a gas-measuring burette (precision of 0.1 mL) was used. A closed vessel containing a solution of catalyst was stirred at constant temperature on a water bath. Previously thermostated H_2O_2 ($[H_2O_2]$: [catalyst] ratio 130–375 : 1) was injected through a silicon stopper, and the evolved dioxygen was volumetrically measured. Blank experiments performed in an Et_3N–$Et_3NH\cdot ClO_4$ buffer (pH = 11) without the catalyst showed that after 40 min only 5% of the initial H_2O_2 had disproportionated, while when the catalyst was present, all H_2O_2 decomposed in less than 3 min.

Kinetic measurements

Oxygen evolution studies were carried out polarographically using a Clark-type oxygen electrode with an YSI oxygen-monitoring system (Model 5300, Yellow Springs Instruments Co., Inc.). The initial rate method was used to determine the rate constants (see ref. 24 for further details). Each rate constant reported here represents the mean value of multiple determinations that fall within ±5%. Experiments were carried out at 25 °C.

Acknowledgements

We thank the National University of Rosario and CONICET for financial support.

References

1 M. Shank, V. Barynin and G. C. Dismukes, *Biochemistry*, 1994, **33**, 15433–15436.
2 J. E. Penner-Hahn and V. L. Pecoraro, in *Manganese Redox Enzymes*, ed. V. L. Pecoraro, VCH, New York, 1992, p. 29, 197.
3 J. Mizobata, M. Kagawa, N. Murakoshi, E. Kusaka, K. Kameo, Y. Kawata and J. Nagai, *Eur. J. Biochem.*, 2000, **267**, 4264–4271.
4 J. E. Penner-Hahn, in *Manganese Redox Enzymes*, ed. V. L. Pecoraro, VCH, New York, 1992, pp. 29–45.
5 T. Amo, H. Atomi and T. Imanaka, *J. Bacteriol.*, 2002, **184**, 3305–3312.
6 M. Bernroitner, M. Zamocky, P. G. Furtmüller, G. A. Peschek and C. Obinger, *J. Exp. Bot.*, 2009, **60**, 423–440.
7 S. V. Antonyuk and V. V. Barynin, *Crystallogr. Rep.*, 2000, **45**, 105–116.
8 V. V. Barynin, M. M. Whittaker, S. V. Antonyuk, V. S. Lamzin, P. M. Harrison, P. J. Artymiuk and J. W. Whittaker, *Structure*, 2001, **9**, 725–738.
9 A. J. Wu, J. E. Penner-Hahn and V. L. Pecoraro, *Chem. Rev.*, 2004, **104**, 903–938.
10 J. W. De Boer, W. R. Browne, B. L. Feringa and R. Hage, *C. R. Chim.*, 2007, **10**, 341–354.
11 S. Signorella, J. P. Tuchagues, D. Moreno and C. Palopoli, in *Inorganic Biochemistry Research Progress*, ed. J. G. Hughes and A. J. Robinson, Nova Science Publishers Inc., New York, 2008, pp. 243–279.
12 S. Signorella and C. Hureau, *Coord. Chem. Rev.*, 2012, **256**, 1229–1245.
13 M. M. Whittaker, V. V. Barynin, T. Igarashi and J. W. Whittaker, *Eur. J. Biochem.*, 2003, **270**, 1102–1116.
14 M. Kagawa, N. Murakoshi, Y. Nishikawa, G. Matsumoto, Y. Kurata, T. Mizobata, Y. Kawata and J. Nagai, *Arch. Biochem. Biophys.*, 1999, **362**, 346–355.
15 B. K. Shin, M. Kim and J. Han, *Polyhedron*, 2010, **29**, 2560–2568.
16 J. A. Lessa, A. Horn Jr., E. S. Bull, M. R. Rocha, M. Benassi, R. R. Catharino, M. N. Eberlin, A. Casellato, C. J. Noble, G. R. Hanson, G. Schenk, G. C. Silva, O. A. C. Antunes and C. Fernandes, *Inorg. Chem.*, 2009, **48**, 4569–4579.
17 S. R. Doctrow, K. Huffman, C. B. Marcus, G. Tocco, E. Malfroy, C. A. Adinolfi, H. Kruk, K. Baker, N. Lazarowych, J. Mascarenhas and B. Malfroy, *J. Med. Chem.*, 2002, **45**, 4549–4558.
18 Y. Nishida, T. Akamatsu, K. Tsuchiya and M. Sakamoto, *Polyhedron*, 1994, **13**, 2251–2254.
19 I. Kani, C. Darak, O. Sahin and O. Büyükgüngör, *Polyhedron*, 2008, **27**, 1238–1247.
20 C. Palopoli, N. Bruzzo, C. Hureau, S. Ladeira, D. Murgida and S. Signorella, *Inorg. Chem.*, 2011, **50**, 8973–8983.
21 W.-T. Lee, S. Xu, D. A. Dickie and J. M. Smith, *Eur. J. Inorg. Chem.*, 2013, 3867–3873.
22 M. R. Bermejo, A. Castiñeiras, J. C. Garcia-Monteagudo, M. Rey, A. Sousa, M. Watkinson, C. A. McAuliffe, R. G. hitchard and R. L. Beddoes, *J. Chem. Soc., Dalton Trans.*, 1996, 2935–2944.
23 K. Nakamoto, *Infrared and Raman Spectra of Inorganic and Coordination Compounds*, Wiley-Interscience, New York, 5th edn, 1997, Part B, p. 60.
24 C. Palopoli, B. Chansou, J. P. Tuchagues and S. Signorella, *Inorg. Chem.*, 2000, **39**, 1458–1462.

25 H. Biava, C. Palopoli, S. Shova, M. De Gaudio, V. Daier, M. González-Sierra, J. P. Tuchagues and S. Signorella, *J. Inorg. Biochem.*, 2006, **100**, 1660–1671.

26 D. Moreno, C. Palopoli, V. Daier, S. Shova, L. Vendier, M. González-Sierra, J. P. Tuchagues and S. Signorella, *Dalton Trans.*, 2006, 5156–5166.

27 V. Daier, H. Biava, C. Palopoli, S. Shova, J. P. Tuchagues and S. Signorella, *J. Inorg. Biochem.*, 2004, **98**, 1806–1817.

28 C. Palopoli, M. González-Sierra, G. Robles, F. Dahan, J. P. Tuchagues and S. Signorella, *J. Chem. Soc., Dalton Trans.*, 2002, 3813–3819.

29 E. Larson, M. S. Lah, X. Li, J. A. Bonadies and V. L. Pecoraro, *Inorg. Chem.*, 1992, **31**, 373–378.

30 M. Mikuriya, N. Torihara, H. Okawa and S. Kida, *Bull. Chem. Soc. Jpn.*, 1981, **54**, 1063–1067.

31 A. Gelasco, M. L. Kirk, J. W. Kampf and V. L. Pecoraro, *Inorg. Chem.*, 1997, **36**, 1829–1837.

32 M. Mikuriya, Y. Yamato and T. Tokii, *Bull. Chem. Soc. Jpn.*, 1992, **65**, 1466–1468.

33 Z. Zhang, C. Brouca-Cabarrecq, C. Hemmert, F. Dahan and J.-P. Tuchagues, *J. Chem. Soc., Dalton Trans.*, 1995, 1453–1460.

34 J. J. Zhang, Q. H. Luo, C. Y. Duan, Z. L. Wang and Y. H. Mei, *J. Inorg. Biochem.*, 2001, **86**, 573–579.

35 H. Miyasaka, R. Clérac, W. Wernsdorfer, L. Lecren, C. Bonhomme, K. I. Sugiura and M. Yamashita, *Angew. Chem., Int. Ed.*, 2004, **43**, 2801–2805.

36 L. Dubois, D. F. Xiang, S. S. Tan, J. Pecaut, P. Jones, S. Baudron, L. Le Pape, J. M. Latour, C. Baffer, S. Chardon-Noblat, M. N. Collomb and A. Deronzier, *Inorg. Chem.*, 2003, **42**, 750–760.

37 P. Karsten, A. Neves, A. Bortoluzzi, J. Strähle and C. Maichle-Mössmer, *Inorg. Chem. Commun.*, 2002, **5**, 434–438.

38 A. Neves, S. M. D. Erthal, I. Vencato, A. S. Ceccato, Y. P. Mascarehas, O. R. Nascimento, M. Hörner and A. A. Batista, *Inorg. Chem.*, 1992, **31**, 4749–4755.

39 M. Hirotsu, M. Kojima, W. Mori and Y. Yoshikawa, *Bull. Chem. Soc. Jpn.*, 1998, **71**, 2873–2884.

40 C. Hureau, E. Anxolabéhère-Mallart, M. Nierlich, F. Gonnet, E. Rivière and G. Blondin, *Eur. J. Inorg. Chem.*, 2002, 2710–2719.

41 C. Hureau, L. Sabater, E. Anxolabéhère-Mallart, M. Nierlich, M.-F. Charlot, F. Gonnet, E. Rivière and G. Blondin, *Chem. – Eur. J.*, 2004, **10**, 1998–2010.

42 J. Bonadies, M. Maroney and V. L. Pecoraro, *Inorg. Chem.*, 1989, **28**, 2044–2051.

43 M. T. Caudle, P. Riggs-Gelasco, A. K. Gelasco, J. E. Penner-Hahn and V. L. Pecoraro, *Inorg. Chem.*, 1996, **35**, 3577–3584.

44 M. R. Bermejo, A. M. González, M. Fondo, A. García-Deibe, M. Maneiro, J. Sanmartín, O. Hoyos and M. Watkinson, *New J. Chem.*, 2000, **24**, 235–241.

45 M. R. Bermejo, A. M. González-Noya, V. Abad, M. I. Fernández, M. Maneiro, R. Pedrido and M. Vásquez, *Eur. J. Inorg. Chem.*, 2004, 3696–3705.

46 A. E. M. Boelrijk, S. V. Khangulov and G. C. Dismukes, *Inorg. Chem.*, 2000, **39**, 3009–3019.

47 E. J. Larson and V. L. Pecoraro, *J. Am. Chem. Soc.*, 1991, **113**, 7809–7810.

48 J. A. Bonadies, M. L. Kirk, M. S. Lah, D. P. Kessissoglou, W. E. Hatfield and V. L. Pecoraro, *Inorg. Chem.*, 1989, **28**, 2037–2044.

49 E. J. Larson and V. L. Pecoraro, *J. Am. Chem. Soc.*, 1991, **113**, 3810–3818.

50 G. Berggren, P. Huang, L. Eriksson, S. Styring, M. F. Anderlung and A. Thapper, *Dalton Trans.*, 2010, **39**, 11035–11044.

51 A. E. M. Boelrijk and G. C. Dismukes, *Inorg. Chem.*, 2000, **39**, 3020–3028.

52 K. J. Berry, F. Moya, K. S. Murray, A. M. B. Bergen and B. O. West, *J. Chem. Soc., Dalton Trans.*, 1982, 109–116.

53 M. Botsivali, D. F. Evans, P. H. Missen and M. W. Upton, *J. Chem. Soc., Dalton Trans.*, 1985, 1147–1149.

54 Stoe, *IPDS Manual, Version 2.75, Stoe & Cie*, Darmstadt, Germany, 1996.

55 Stoe, *X-RED, Data Reduction for STADI4 and IPDS, Revision 1.08, Stoe & Cie*, Darmstadt, Germany, 1996.

56 A. Altomare, G. Cascarano, G. Giacovazzo, A. Guagliardi, M. C. Burla, G. Polidori and M. Camalli, *J. Appl. Crystallogr.*, 1994, **27**, 435.

57 G. M. Sheldrick, *SHELXL-97, Program for the Refinement of crystal structures from diffraction data*, University of Göttingen, Göttingen, Germany, 1997.

58 L. J. Farrugia, *J. Appl. Crystallogr.*, 1997, **30**, 565.

59 I. Murase, M. Hatano, M. Tanaka, S. Ueno, H. Okawa and S. Kida, *Bull. Chem. Soc. Jpn.*, 1982, **55**, 2404–2408.